Geophys. J. R. astr. Soc. (1977) **49**, 181–208

Seismic body waves in anisotropic media: reflection and refraction at a plane interface

Colum M. Keith* *Department of Geophysics, University of Edinburgh, James Clerk Maxwell Building, Edinburgh EH9 3JZ*

Stuart Crampin *Institute of Geological Sciences, Murchison House, West Mains Road, Edinburgh EH9 3LA*

Received 1976 May 10

Summary. A formulation is derived for calculating the energy division among waves generated by plane waves incident on a boundary between generally anisotropic media. A comprehensive account is presented for *P*, *SV* and *SH* waves incident from an isotropic half-space on an orthorhombic olivine half-space, where the interface is parallel to a plane of elastic symmetry. For comparison, a less anisotropic medium having transverse isotropy with a horizontal axis of symmetry is also considered. The particle motion polarizations of waves in anisotropic medium differ greatly from the polarizations in isotropic media, and are an important diagnostic of the presence of anisotropy. Incident *P* and *SV* waves generate quasi-*SH* waves, and incident *SH* waves generate quasi-*P* and quasi-*SV* waves, often of considerable relative magnitude. The direction of energy transport diverges from the propagation direction.

1 Introduction

Time-term refraction studies have shown that the mantle beneath the Moho exhibits velocity anisotropy under oceans (Raitt *et al.* 1969, 1971) and under continents (Bamford 1973; Berry & Fuchs 1974). This velocity anisotropy is considered to be due to alignment of olivine crystals (Hess 1964; Francis 1969). Observations of anomalous surface-wave particle motion, diagnostic of the presence of anisotropy, have been made by Crampin (1966, 1967), and Crampin & King (1977), in studies of higher mode surface waves propagating across Eurasia.

Many of the theoretical discussions of anisotropy in seismology have been about transverse isotropy with a vertical axis of symmetry. In such a structure there is no azimuthal variation. Crampin (1970, 1975), and Crampin & Taylor (1971) investigated numerically surface-wave propagation in anisotropic media by a generalized technique permitting any

* Present address: Department of Energy, Mines and Resources, Ottawa, Ontario, Canada.

combination of plane layers possessing any anisotropic symmetry. There is no such computational work available for body-wave propagation, although a number of theoretical formulations have been suggested, including an asymtotic ray approximation by Cerveny (1972).

In this paper we present an account of the reflection and refraction of plane body waves at a boundary between an isotropic and an anisotropic half-space; thus investigating the behaviour of teleseismic body waves incident (say) on an anisotropic upper mantle from an isotropic lower mantle, and demonstrating many of the effects of the interactions at an isotropic/anisotropic interface. It seems likely that forces orienting crystals in the upper mantle would result in the anisotropy having a horizontal plane of symmetry, and all the models used for the numerical calculations have a plane of elastic symmetry parallel to the interface.

This study of simple reflection and refraction at an isotropic/anisotropic interface is, we believe, a necessary prelude to computations on more realistic structures, if we are to retain any intuitive understanding of the processes involved.

2 Mathematical formulation

The technique we present here is a general theory based on Synge (1956, 1957) and Crampin (1970). The equations of motion of free vibration of an elastic medium are

$$\left(\rho\,\delta_{jm}\,\frac{\partial^2}{\partial t^2} - c_{jkmn}\,\frac{\partial^2}{\partial x_k\,\partial x_n}\right)u_m = 0, \quad j = 1, 2, 3 \tag{1}$$

where $\boldsymbol{u}$ is the displacement, ρ the density, c_{jkmn} the tensor of elastic constants, δ_{jm} is the Kronecker delta function, and the summation convention is understood. We seek plane harmonic solutions of the form

$$u_j = a_j \exp\left[i\omega(t - q_k\,x_k)\right], \quad j = 1, 2, 3 \tag{2}$$

where $\boldsymbol{a}$ is the polarization vector, ω the angular frequency, and $\boldsymbol{q}$ the slowness vector. Substituting the displacements in the equations of motions, we have three equations

$$\rho\,a_j = c_{jkmn}\,q_k\,q_n\,a_m, \quad j = 1, 2, 3 \tag{3}$$

For non-zero $\boldsymbol{a}$ we require

$$\det\,(F_{jm}) = 0, \tag{4}$$

where

$$F_{jm} = -\rho\,\delta_{jm} + c_{jkmn}\,q_k\,q_n, \quad j, m = 1, 2, 3 \tag{5}$$

The displacements (2) are a solution provided the slowness vector satisfies equation (4). These slowness vectors trace out a three-sheeted surface called the slowness surface. Fig. 1 shows a section of such a surface. The three sheets correspond to three propagating body waves for a given direction. For an isotropic medium these sheets are spheres and the two sheets corresponding to the transverse waves are coincident. For anisotropic media these sheets are in general separate and non-spherical. Only the inner sheet is necessarily convex.

The polarization vectors defined by equation (3) are orthogonal, but in general not coincident with the dynamic axes defined by the propagation vector and plane of constant phase. In isotropic media, the polarization vectors of the S waves can be in any two

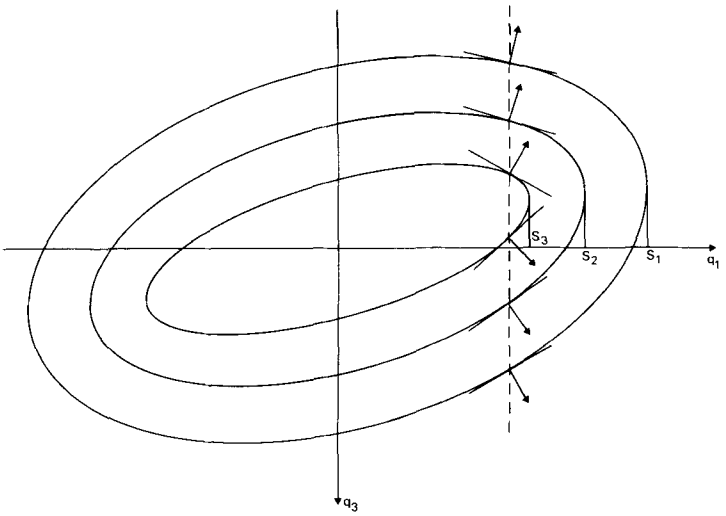

Figure 1. A section of a possible slowness surface. For a given slowness $q_1 < S_3$, the intersection of the dotted line with each body wave surface maps out six real values of q_3. As q_1 increases beyond each S_i, the corresponding pair of q_3 roots becomes complex.

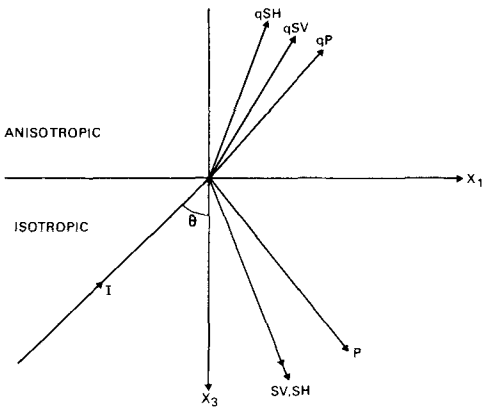

Figure 2. I is the propagation vector of the incident wave. P, SV, and SH are the propagation vectors of the reflected waves and qP, qSV, and qSH are the propagation vectors of the transmitted waves. θ is the angle of incidence.

orthogonal transverse directions. In anisotropic media this degeneracy is removed, and the polarization vectors, determined by equation (3), are mutually orthogonal, and are fixed in the solid, dependent only on the direction of propagation (Keith 1975; Crampin 1977).

The notation is shown in Fig. 2, where we rotate the elastic tensor by the usual tensor transformation so that the plane $x_2 = 0$ contains the propagation vector incident at an angle θ on the interface $x_3 = 0$. Without loss of generality we take $q_1 = 1/c$ and $q_2 = 0$, where c is the apparent phase velocity along the interface, $c = v/\sin\theta$, and v is the phase velocity of the plane wave. The arrows of the transmitted waves in the anisotropic medium in Fig. 2, do not represent rays, that is directions of energy transport. They represent the directions of the propagation vectors at the interface. As a consequence of the velocity anisotropy, the propagation of energy at the group velocity diverges from the propagation vector (Crampin

1977) and, in particular, is not in the plane of incidence unless this plane is one of elastic symmetry.

The slowness equation (4) is now a sextic polynomial in q (dropping the subscript 3) with real coefficients. Solutions are either real, corresponding to propagating body waves, or in complex conjugate pairs, corresponding to inhomogeneous waves tied to the interface. Fig. 1 shows a situation where there are six real roots. The direction of propagation of the waves corresponding to these roots are given by the directions of the normals to the slowness surface at these points. Three roots correspond to upward and three to downward propagating waves. We order the six roots, $q(n), n = 1, \ldots, 6$, such that $n = 1, 2, 3$, correspond to downward (positive z direction) travelling quasi-longitudinal and two quasi-transverse waves, respectively, and $n = 4, 5, 6$, to upward travelling quasi-transverse and quasi-longitudinal waves, respectively.

The polarization vector a can be obtained from the solution of equation (4)

$$\frac{a_1(n)}{\begin{vmatrix} F_{22}(n) & F_{23}(n) \\ F_{32}(n) & F_{33}(n) \end{vmatrix}} = \frac{a_2(n)}{\begin{vmatrix} F_{23}(n) & F_{21}(n) \\ F_{33}(n) & F_{33}(n) \end{vmatrix}} = \frac{a_3(n)}{\begin{vmatrix} F_{21}(n) & F_{22}(n) \\ F_{31}(n) & F_{32}(n) \end{vmatrix}} \qquad n = 1, \ldots, 6 \tag{6}$$

The extra degree of freedom is removed by normalizing the vectors.

We can now write a general solution in the form

$$u_j = \sum_{n=1}^{6} f(n) a_j(n) \exp\left[i\omega(t - x_1/c - q(n)x_3)\right], \quad j = 1, 2, 3, \tag{7}$$

where the f are relative excitation factors. At an interface both traction and displacement are continuous. We define a tensor t_{jk} related to the stress tensor p_{jk} by

$$t_{jk} = p_{jk} \frac{ic}{\omega}, \quad j, k, = 1, 2, 3 \tag{8}$$

The components of this tensor are given by

$$t_{jk} = \sum_{n=1}^{6} f(n) a_m(n) (c_{jkm1} + c_{jkm3} c q(n)) \cdot \exp\left[i\omega(t - x_1/c - q(n)x_3)\right], \quad j, k = 1, 2, 3 \tag{9}$$

The six-vector of excitation factors in (9) is related to the displacement-stress six-vector

$$\mathbf{v}^{\mathrm{T}} = (u_1, u_2, u_3, t_{31}, t_{32}, t_{33})$$

at the interface by

$$\mathbf{v} = E_2 \mathbf{f}_2 \tag{10}$$

where the 6 x 6 matrix E_2 for the lower half-space has components

$$\begin{aligned} E_{jn} &= a_j(n), && j = 1, 2, 3, && n = 1, \ldots, 6 \\ &= a_m(n)(c_{j3m1} + c_{j3m3} c q(n)), && j = 4, 5, 6 && n = 1, \ldots, 6 \end{aligned} \tag{11}$$

A similar matrix relates the displacement-stress vector at the interface to the excitation factors in the upper half-space by

$$\mathbf{v} = E_1 \mathbf{f}_1 \tag{12}$$

Combining (10) and (12) we have

$$\mathbf{f}_2 = E_2^{-1} E_1 \mathbf{f}_1 = J\mathbf{f}_1 \tag{13}$$

which connects the excitation factors in the upper and lower half-spaces. If a half-space is anisotropic the matrix E must be inverted numerically. If a half-space is isotropic the E matrix has a simple form, whose inverse can be found analytically and is given by Crampin (1970).

For an incident longitudinal wave we set the excitation of the three upward travelling waves in the lower half-space as $f(4)=f(5)=0$ and $f(6)=1$. There are no downward travelling waves in the upper half-space, and $f(1)=f(2)=f(3)=0$. In matrix form equation (13) is thus

$$(f(1), f(2), f(3), 0, 0, 1)_2^{\mathrm{T}} = J(0, 0, 0, f(4), f(5), f(6))_1^{\mathrm{T}}, \tag{14}$$

which can be solved for the unknown excitation factors and hence for the amplitudes of the reflected and transmitted waves.

We note here that the boundary conditions at the interface, continuity of displacements and stresses, is important as an aid to intuitive understanding. The continuity of the particle displacements provides an insight into the anomalous behaviour at interfaces.

To obtain the energy ratios we use the expression for the energy flux vector of a given wave (Synge 1956)

$$F_j = \tfrac{1}{4}\omega^2 ff^* c_{jkmn}(a_k^* q_m a_n + a_k q_m^* a_n^*), \quad j=1,2,3 \tag{15}$$

for both propagating and inhomogeneous waves, where the asterisk denotes the complex conjugate. For propagating waves, both $\boldsymbol{q}$ and $\boldsymbol{a}$ are real and equation (15) reduces to

$$F_j = \tfrac{1}{2}\omega^2 ff^* c_{jkmn} a_k q_m a_n, \quad j=1,2,3 \tag{16}$$

In isotropic media (15) becomes

$$F_j = \tfrac{1}{2}\omega^2 ff^* \mu q_j$$

for transverse waves and

$$F_j = \tfrac{1}{2}\omega^2 ff^* (\lambda + 2\mu) q_j$$

for longitudinal waves.

Taking $\mathbf{F}^i$, $i=1,2,3$, as the energy flux vectors of the transmitted waves, $\mathbf{F}^i$, $i=4,5,6$, as the energy flux vectors of the reflected waves, and $\mathbf{F}^I$ as the energy flux of the incident wave we can write the conservation of energy requirement as

$$|F_3^I| = \sum_{n=1}^{6} |F_3^n|, \tag{17}$$

where the 3 denotes the x_3 component. Dividing by $|F_3^I|$, we can write this as

$$1 = \sum_{n=1}^{3} (A_n)^2 + \sum_{n=1}^{3} (B_n)^2 \tag{18}$$

where A_1, A_2 and A_3 are the square-root energy ratios of the transmitted waves and B_1, B_2 and B_3 the square-root energies of the reflected waves. We shall present graphs of these square-root energy ratios for angles of incidence between 0° and 90° for various orienta-

tions of the anisotropic material. Energy travels in the direction of the energy flux vector with the group velocity given by

$$\mathbf{U} = \frac{\mathbf{F}}{\mathbf{q} \cdot \mathbf{F}}. \tag{19}$$

3 Reflection and transmission

We present diagrams of the square-root energy ratios of the reflected and transmitted waves generated by *P*, *SV* and *SH* waves incident from an isotropic lower half-space on a half-space of orthorhombic olivine orientated so that a plane of symmetry is parallel to the interface. The velocities of longitudinal waves at atmospheric temperature and pressure along the *a*, *b*, and *c*, crystallographic axes are 9.87, 7.71, and 8.65 km/s, respectively. These velocities and the corresponding velocity anisotropy (*qP* wave maximum of 22 per cent in (001)–plane) are not representative of the upper mantle as observed at the surface, but do illustrate some of the effects produced by anisotropy. To show these effects in a less anisotropic medium we also investigate a transversely isotropic medium with a horizontal axis of symmetry where the velocity variation is 8.6 km/s parallel, and 7.8 km/s perpendicular to the axis (9 per cent velocity anisotropy). The velocities are similar to those observed in the upper mantle. Table 1 shows the elastic constants of these anisotropic media and Table 2 the isotropic half-spaces used in the calculations.

The quasi-longitudinal wave, the fastest anisotropic body wave, will be denoted by *qP*. To distinguish between the quasi-transverse waves we shall denote the one with largest *SV* polarization by *qSV* and the one with largest *SH* polarization by *qSH*. This notation is adequate while we are near planes of symmetry in orthorhombic olivine, but can present difficulties of nomenclature for off-symmetry directions where it is possible for a quasi-

Table 1. (a) Elastic constants of olivine (Verma 1960). (Density = 3.324 g/cm^3.)

$c_{1111} = 324.0$	$c_{2222} = 198.0$	$c_{3333} = 249.0 \times 10^9$ Nm^{-2}
$c_{1122} = 59.0$	$c_{2233} = 78.0$	$c_{3311} = 79.0$
$c_{1212} = 79.0$	$c_{2323} = 66.7$	$c_{1313} = 81.0$

(b) Elastic constants of transversely isotropic medium. (Density = 3.3 g/cm^3.)

$c_{1111} = 260.78$	$c_{2222} = 200.77$	$c_{3333} = 200.77 \times 10^9$ Nm^{-2}
$c_{1122} = 80.0$	$c_{2233} = 72.99$	$c_{3311} = 80.0$
$c_{1212} = 72.9$	$c_{2323} = 63.89$	$c_{1313} = 72.9$

Table 2. Isotropic halfspaces used in the calculations.

Medium	ρ Density g/ cm^3	α km/s	β km/s
1	3.6	10.0	5.77
2	3.6	8.38	4.83
3	3.0	7.5	3.5
4	3.4	8.7	4.8

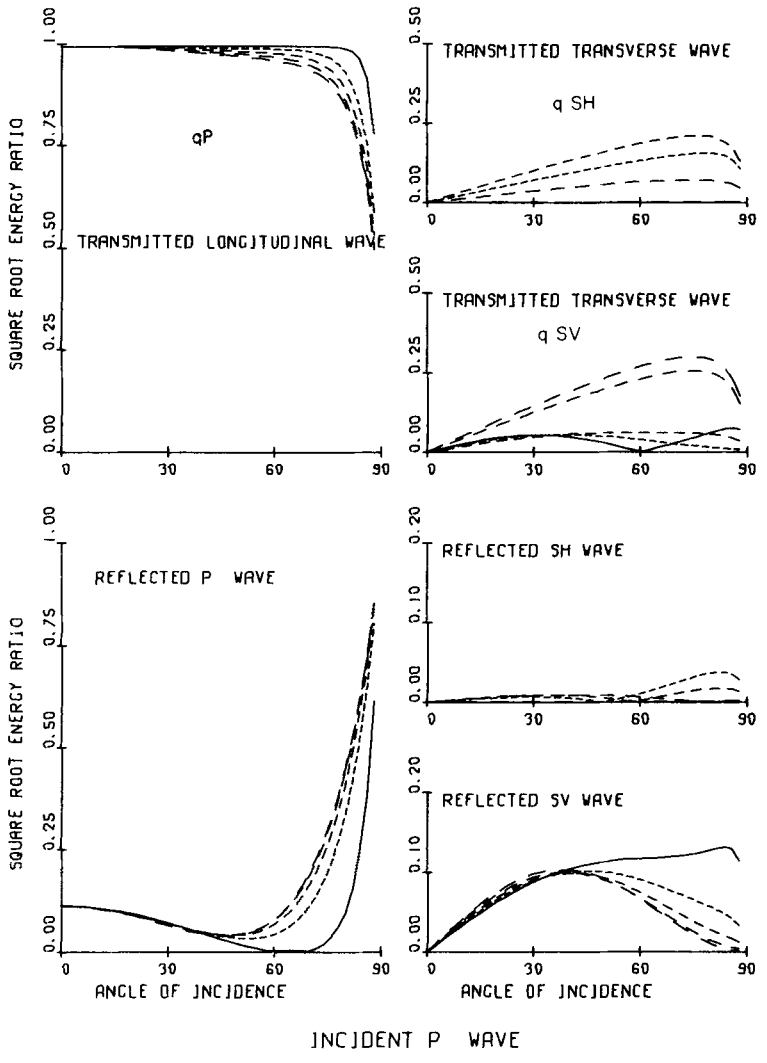

Figure 3(a)

Figure 3. Square-root energy ratios of waves generated at an interface between an isotropic and an anisotropic half-space by plane waves incident from the isotropic half-space, Medium 1 in Table 2. The anisotropic medium is (001)-cut orthorhombic olivine. Orientations of the incident planes on the anisotropic half-space are at 0°, 30°, 45°, 60° and 90° measured from (100) towards (010), and are represented by the continuous line and lines with increasing length of dash, respectively. (a) incident *P* wave, (b) incident *SV* wave and (c) incident *SH* wave. Note that the scales of the axes are not the same in each graph.

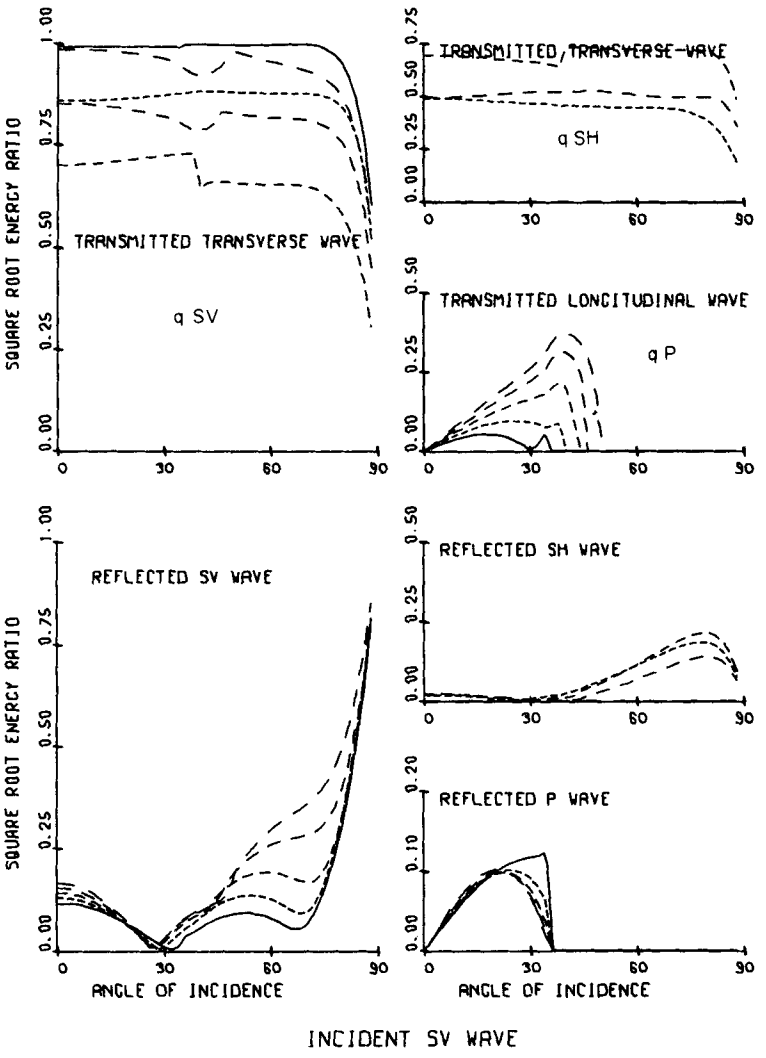

Figure 3(b)

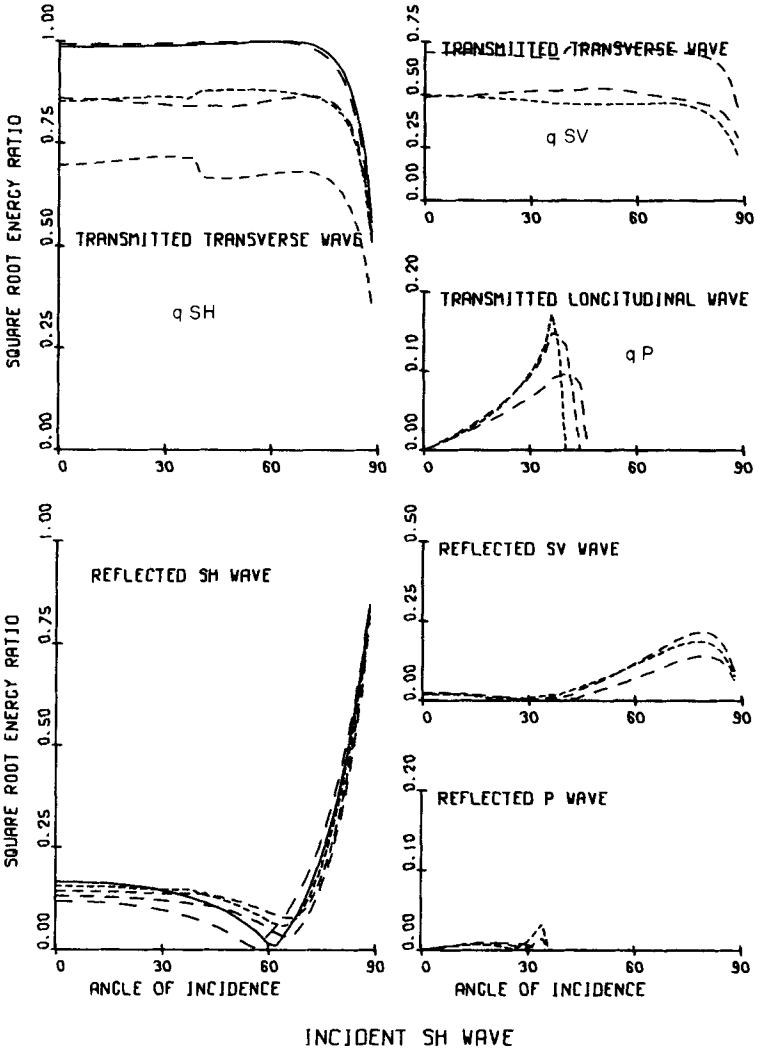

Figure 3(c)

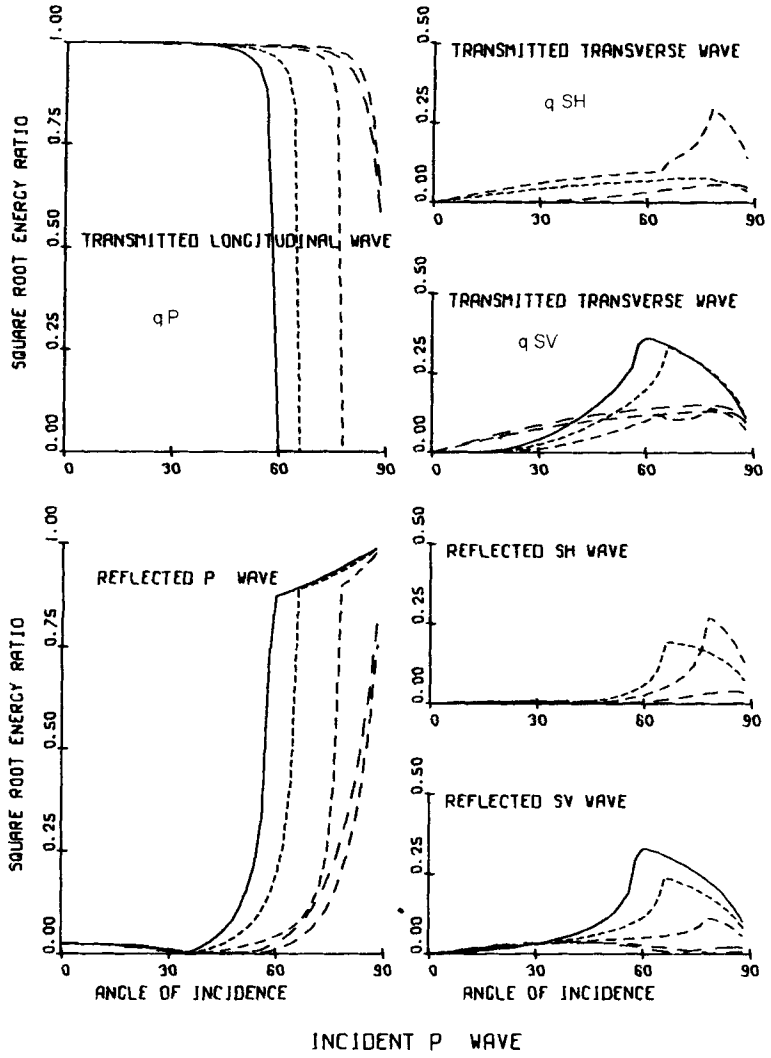

Figure 4(a)

Figure 4. (001)-cut. The orientations are as in Fig. 3. The isotropic half-space is Medium 2. (a) incident *P* wave, (b) incident *SV* wave and (c) incident *SH* wave.

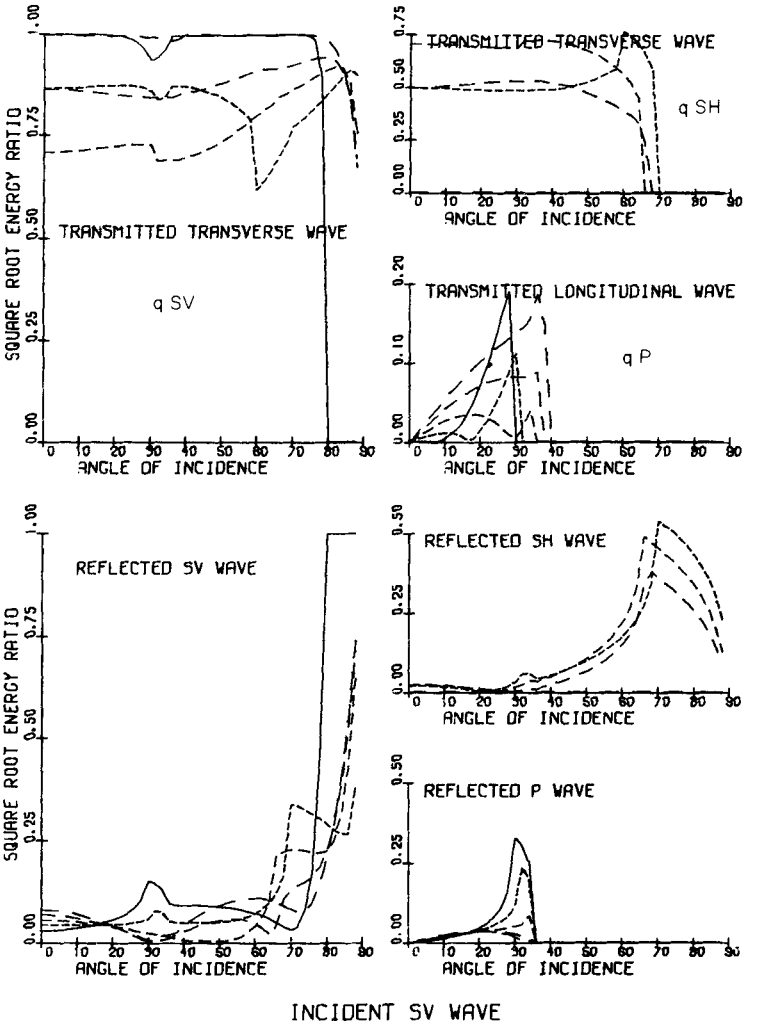

Figure 4 (b)

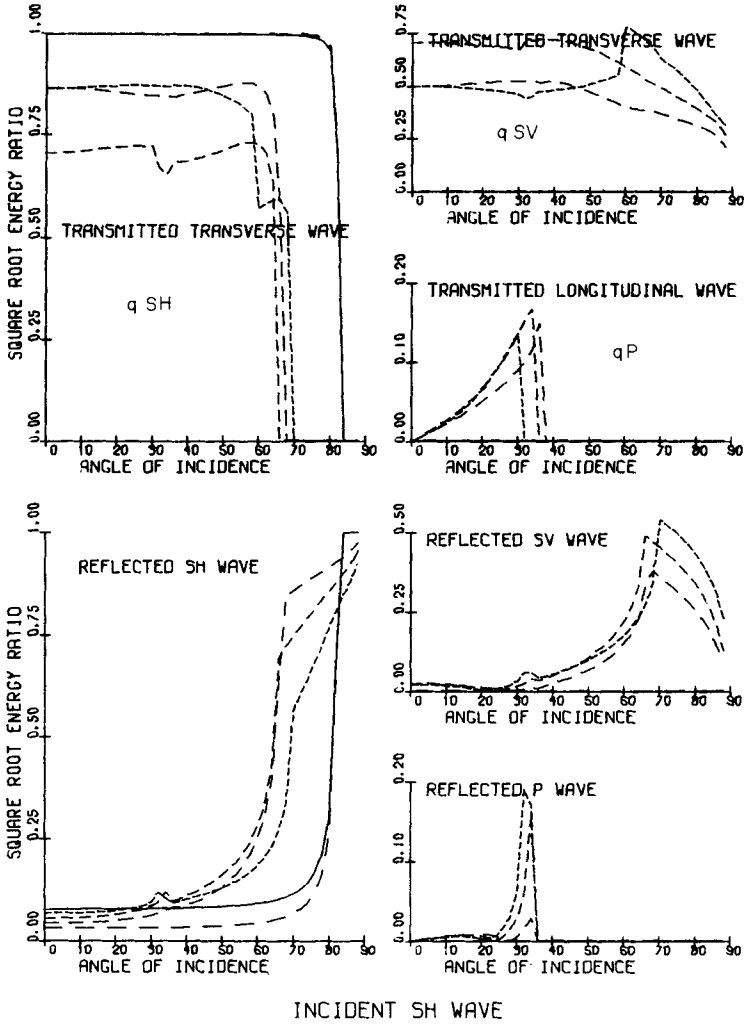

Figure 4 (c)

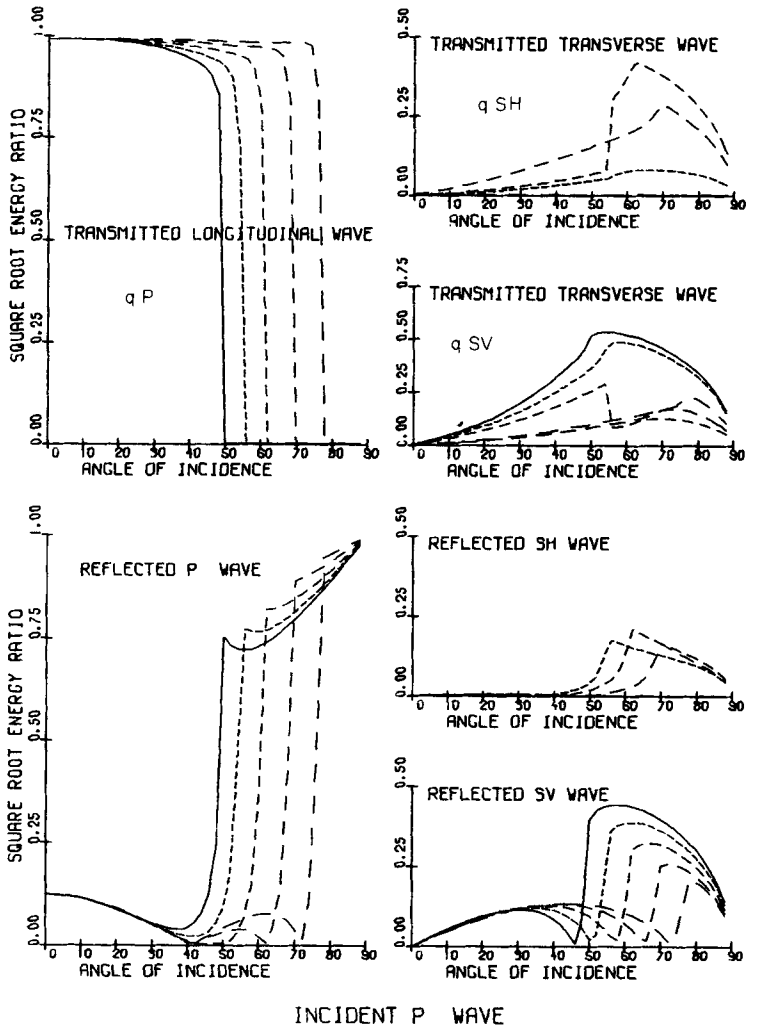

Figure 5(a)

Figure 5. (001)-cut. The orientations are as in Fig. 3. The isotropic half-space is Medium 3. (a) incident *P* wave, (b) incident *SV* wave and (c) incident *SH* wave.

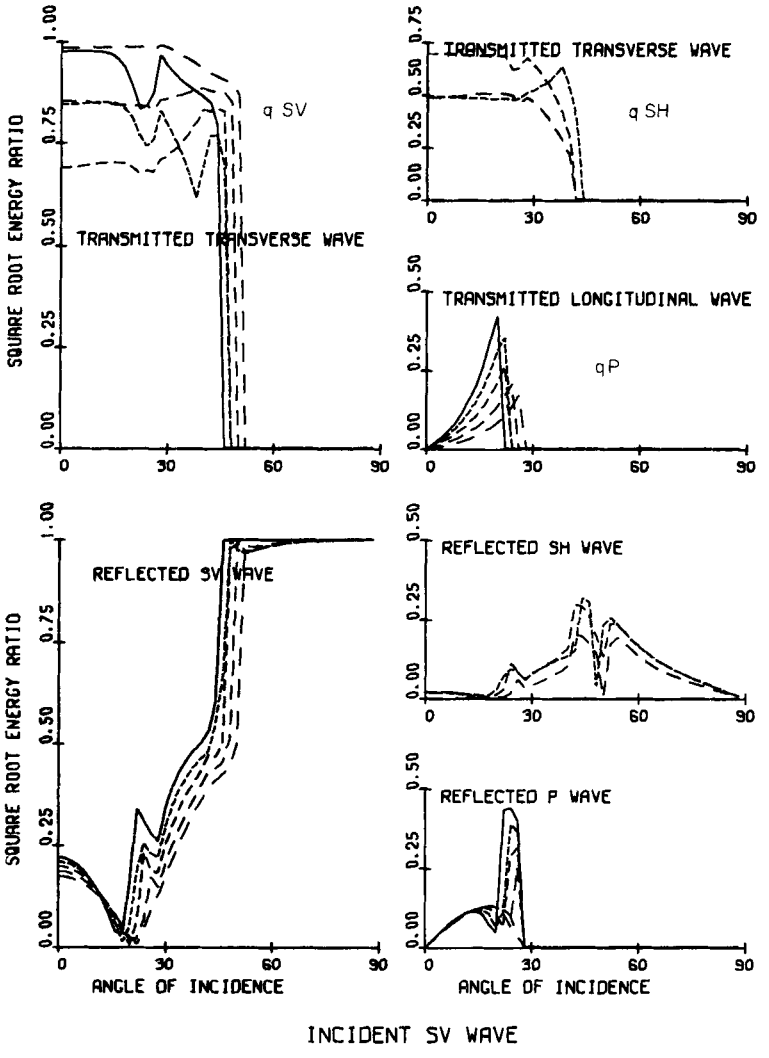

Figure 5(b)

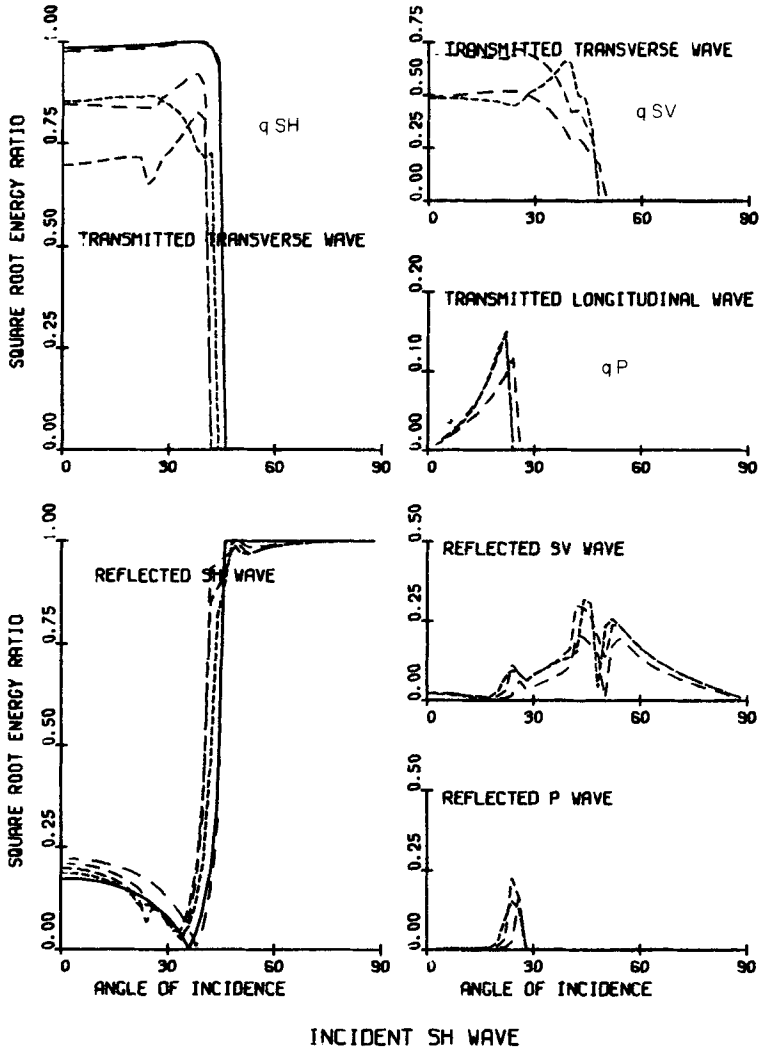

Figure 5(c)

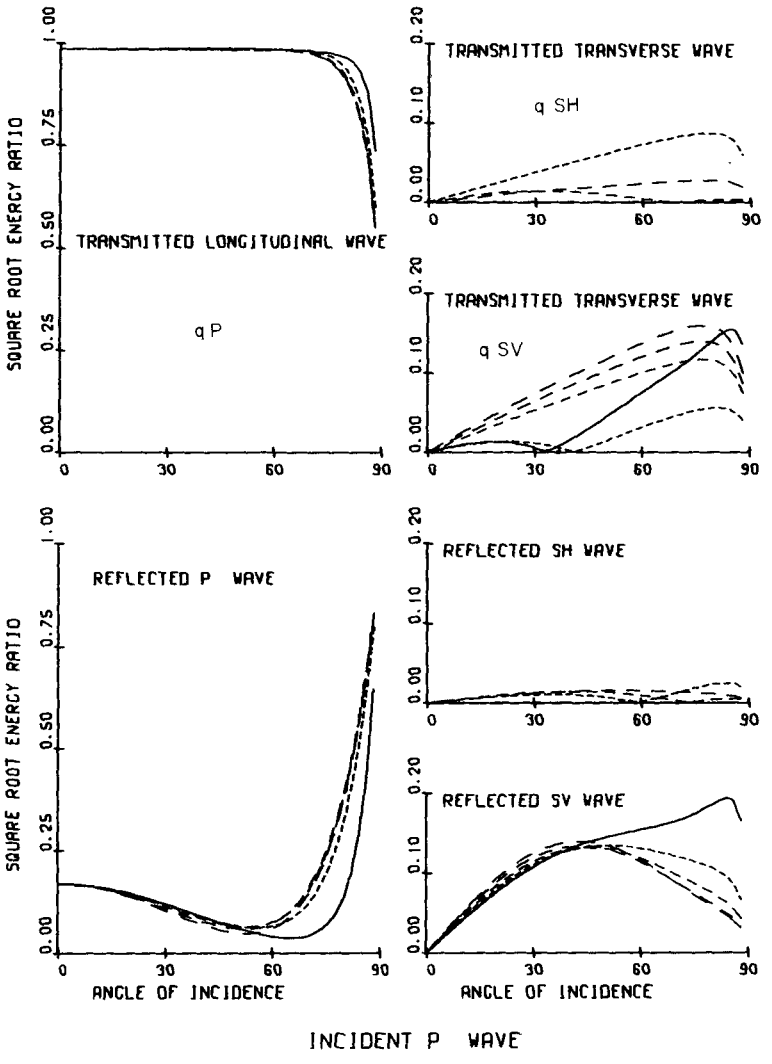

Figure 6(a)

Figure 6. (010)-cut. Orientations of incident plane on the anisotropic half-space are at 0°, 30°, 45°, 60° and 90° measured from (100) towards (001). The isotropic half-space is Medium 1. (a) incident *P* wave, (b) incident *SH* wave.

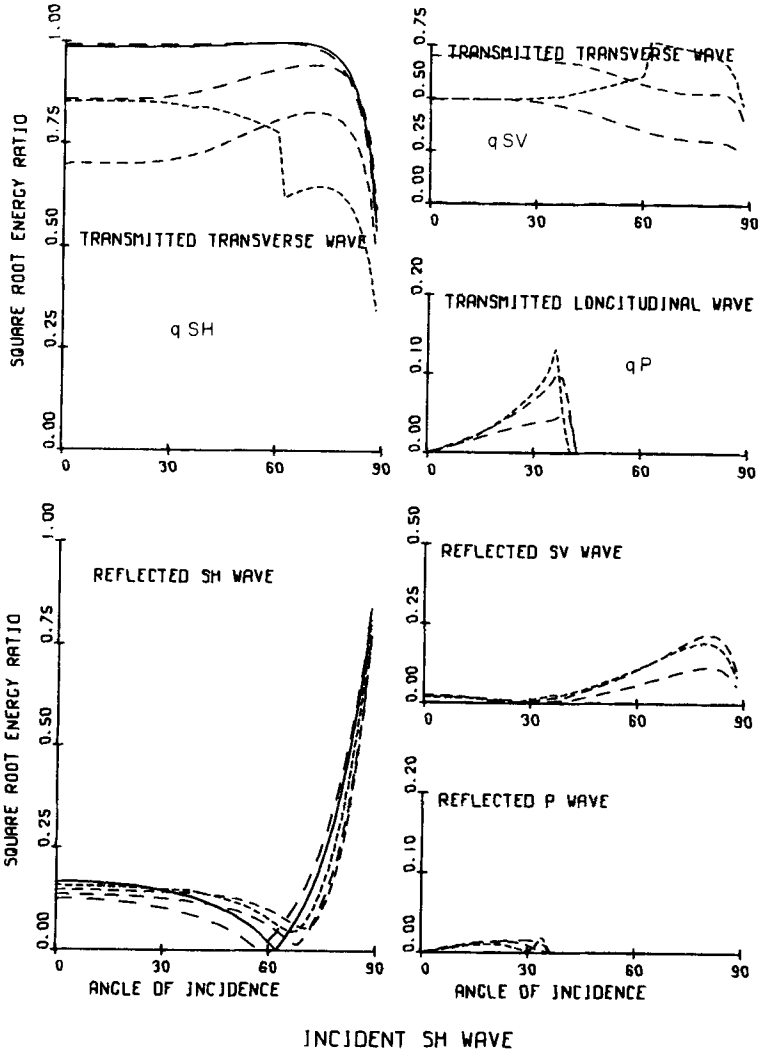

Figure 6(b)

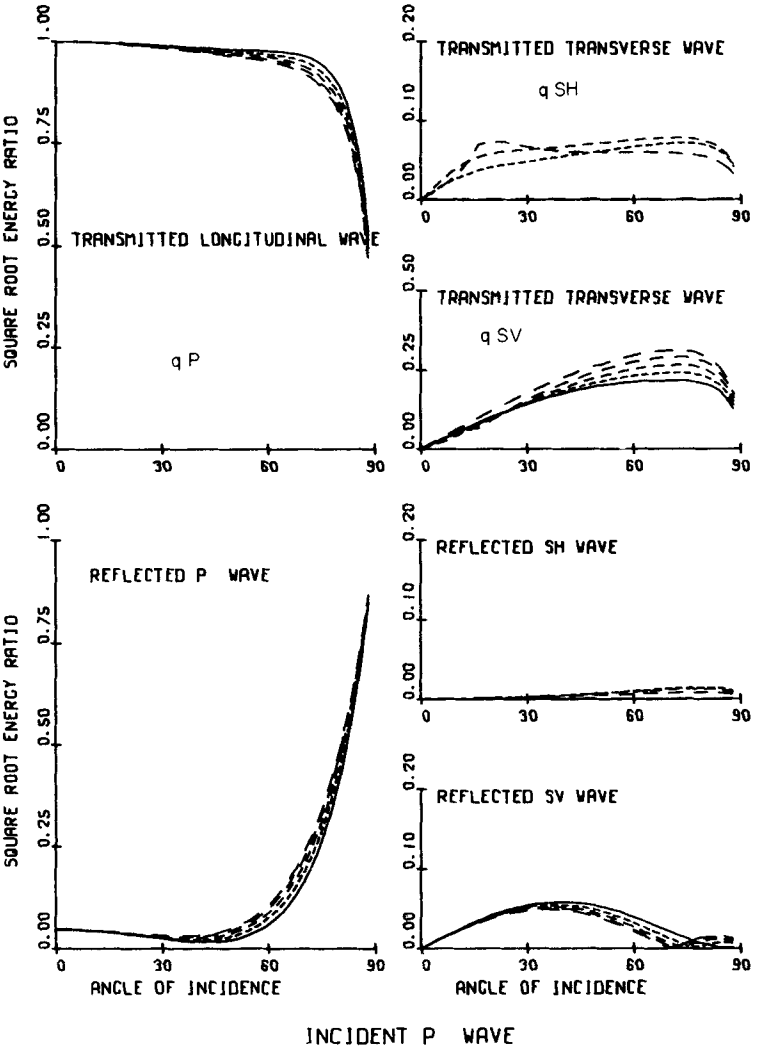

Figure 7(a)

Figure 7. (100)-cut. Orientations of the incident plane on the anisotropic half-space are at 0°, 30°, 45°, 60° and 90° measured from (001) towards (010). The isotropic half-space is Medium 1. (a) incident *P* wave, (b) incident *SV* wave.

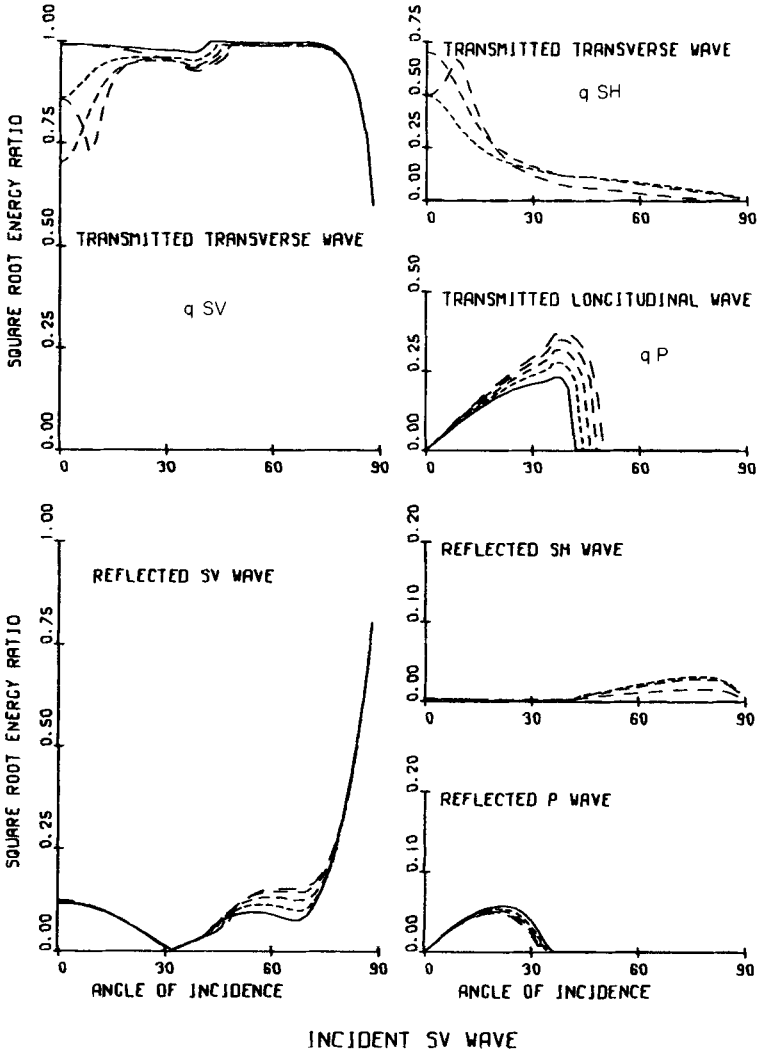

Figure 7(b)

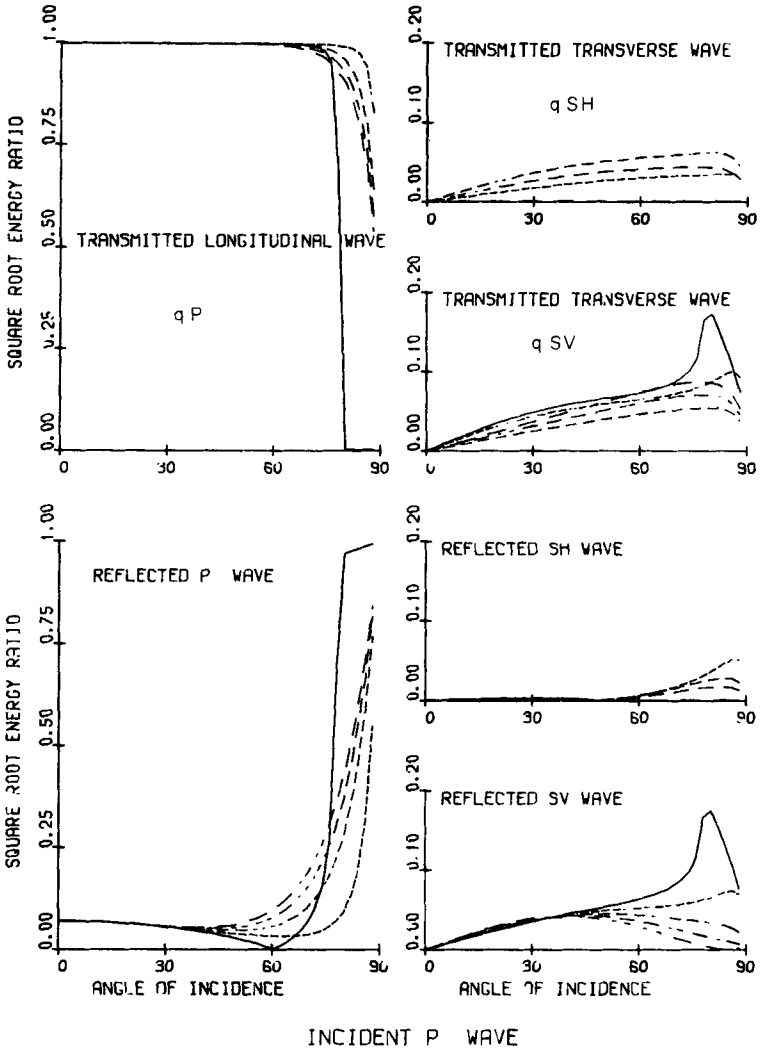

Figure 8(a)

Figure 8. Square-root energy ratios of waves generated at an interface between an isotropic half-space (Medium 4) and a transversely isotropic half-space (Table 1) where the axis of symmetry is parallel to the boundary. The orientations of the incident planes on the anisotropic half-space are at 0°, 30°, 45°, 60° and 90° measured from the axis of symmetry. (a) incident *P* wave, (b) incident *SV* wave and (c) incident *SH* wave.

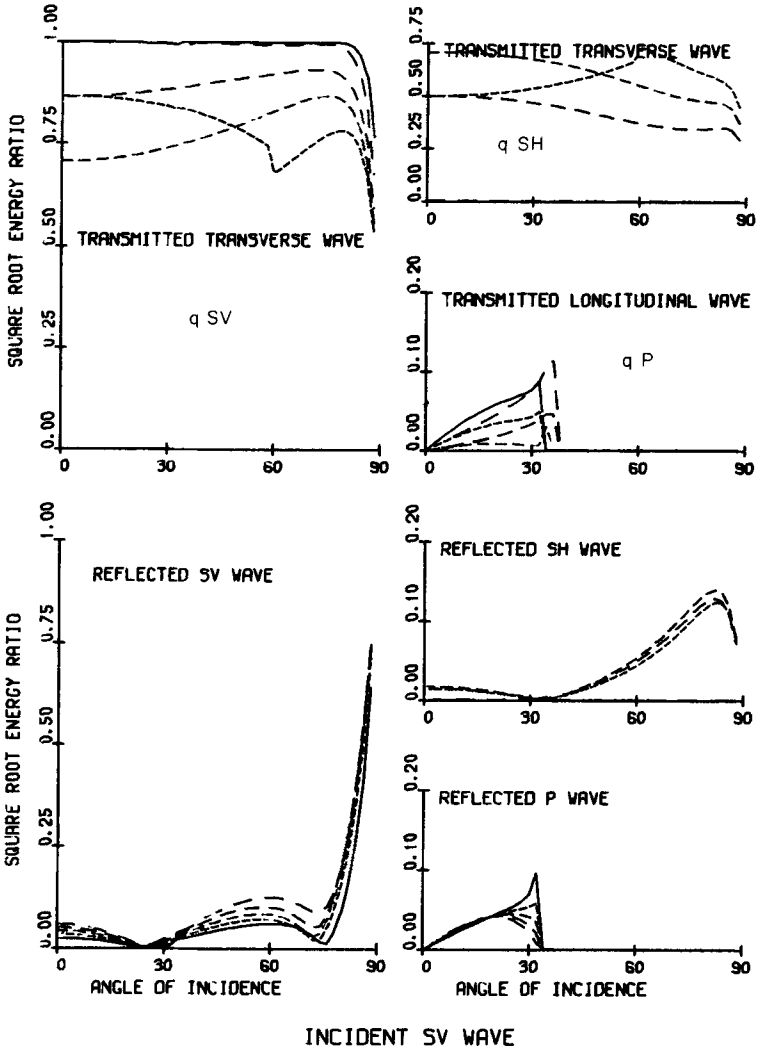

Figure 8(b)

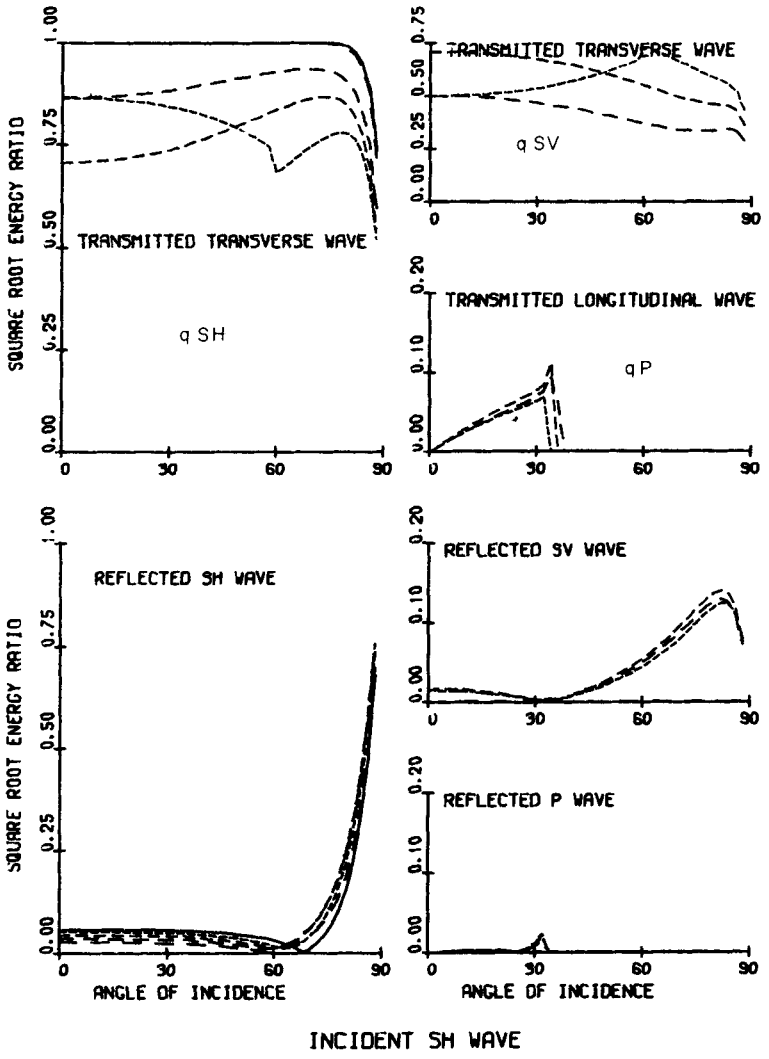

Figure 8(c)

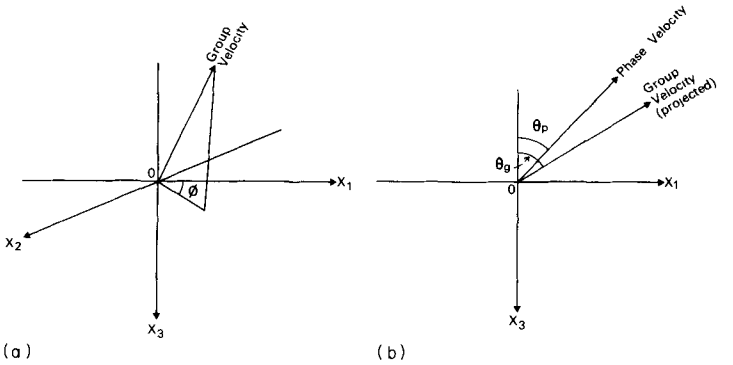

Figure 9. Angles determining group velocity direction. ϕ is the projection of the group velocity refraction angle onto the interface, θ_g is the projection of the group velocity refraction angle onto the incident plane, and θ_p is the phase velocity refraction angle.

transverse wave to vary continuously from *SV* motion to *SH* motion as the direction of propagation changes (Crampin 1977).

Fig. 3(a), (b) and (c) are for *P*, *SV* and *SH* waves, respectively, incident from a lower high-velocity isotropic half-space on (001)-cut olivine. The five curves in each graph are for five orientations of the incident plane.

The two main effects of the anisotropy are apparent in Fig. 3(a) for an incident *P* wave. There is an azimuthal variation in transmission properties, and there are waves present, which are not found in isotropic models. The angle between the particle motion vector of the *qP* wave in the olivine and the propagation direction reaches a maximum of about 15 degrees (Keith 1975), and most of the energy of an incident *P* wave goes into the transmitted *qP* wave. However, whereas in an isotropic medium all the transverse motion required to fit the boundary conditions appears as a transmitted *SV* wave, in the anisotropic case the transverse energy is divided among the two quasi-transverse waves approximately in proportion to the *SV* motion they possess. Thus, for incident planes parallel to an anisotropic plane of symmetry, where one of the quasi-transverse waves has pure *SV* particle motion and the other pure *SH* particle motion, no *qSH* is generated – top right graph in Fig. 3(a). Away from symmetry directions, the *qP* wave polarization has a component of *SH* motion, which does not cancel at the interface, and the transmitted *qSH* energy rises to a smooth maximum between the symmetry directions.

For incident *S* waves, Fig. 3(b) and (c), the behaviour is different. Here the particle motions of neither of the transmitted quasi-transverse waves need be similar to that of the incident wave. Both quasi-transverse waves will be transmitted strongly except for incident planes of symmetry where the particle motions of the transverse waves are pure *SV* and pure *SH*. Consequently no transmitted *qSH* waves exist in Fig. 3(b) and no transmitted *qSV* waves in Fig. 3(c) for such incident planes at 0° and 90°. In general, when the incident plane is away from a plane of symmetry, the motion of the transmitted waves is intermediate between *SV* and *SH* motion and they will be generated by both incident *SV* and *SH* waves. This strong coupling between incident *S* and both quasi-transverse waves is indicated in Fig. 3(b) and (c) by the existence of step discontinuities in the graphs of the transmitted quasi-transverse waves for the 45° orientation of the incident plane at about 40° angle of incidence. At these points the two quasi-transverse waves, as defined, exchange characteristics, i.e. what was the *qSV* wave has become the *qSH* wave and vice versa. Thus the step marks a change in nomenclature, but is not a discontinuity in the physical properties of the waves.

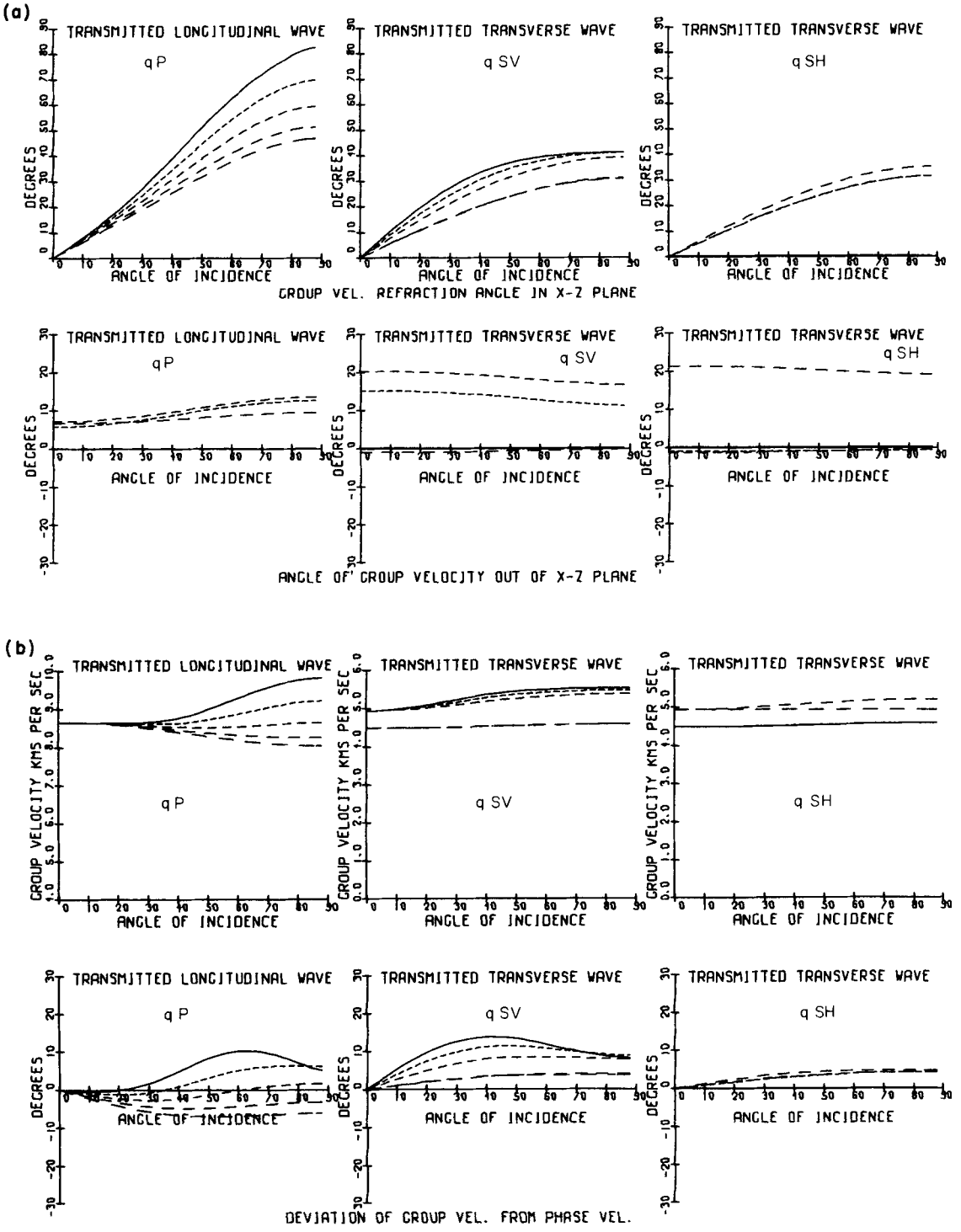

Figure 10. Plots of group velocity angles ϕ and θ_g (Fig. 10(a)), and deviation of group from phase velocity $\theta_g - \theta_p$, and magnitude of group velocity (Fig. 10(b)) for *P* wave incident from isotropic half-space, Medium 1, on (001)-cut olivine. The orientations of the incident planes are at 0°, 30°, 45°, 60° and 90° measured from (100) towards (010).

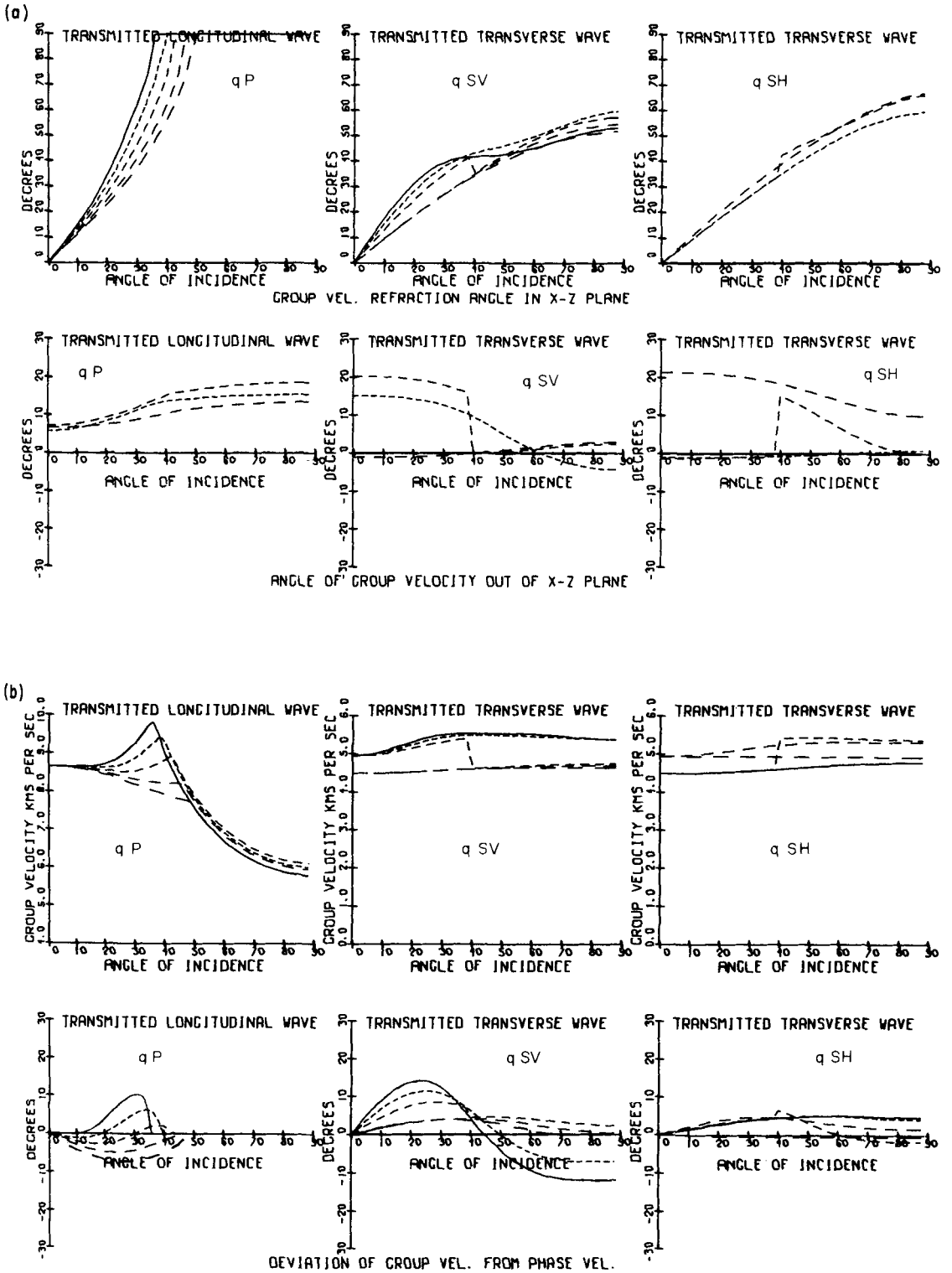

Figure 11. Plots of same quantities as in Fig. 10 for an *SV* wave incident upon the (001)-cut of olivine from Medium 1.

The structure for Fig. 4 is the same as Fig. 3 except that the lower isotropic half-space is a high-velocity medium for some orientations of the anisotropy and a low-velocity medium for others. This is reflected in the *qP* waves in Fig. 4(a) which experience critical angles for some orientations and not others. The transmitted *qSH* wave in Fig. 4(a) is small except for the 45° orientation at 65° angle of incidence where the exchange of *qSV* and *qSH* nomenclature occurs.

Fig. 4(b), for an incident *SV* wave, is complicated by the combined effects of the high-velocity/low-velocity property exhibited in the critical angles, by the interchange of *qSV* and *qSH* nomenclature indicated by the discontinuities in the curves, and by the variation of the coupling of the incident *SV* wave with the transmitted *qSH* wave. The intermediate polarization is emphasized by the many similarities between Fig. 4(b) for an incident *SV* wave and Fig. 4(c) for an incident *SH* wave.

In Fig. 5(a), (b) and (c), the olivine is (001)-cut and the isotropic half-space is a low-velocity medium. An incident *P* wave, Fig. 5(a), experiences a critical angle, which, due to the velocity variation changes value by almost 30° with orientation of the anisotropy. A large-amplitude transmitted *qSH* wave is again caused by the intermediate polarizations of the quasi-transverse waves in the olivine and we again see the importance of the directions of polarization in specifying the propagation of body waves in anisotropic media.

The (010)-cut of olivine exhibits considerably less velocity anisotropy for the *qP* wave than the (001)-cut, but slightly more for the quasi-transverse waves (see Crampin 1977). The effects produced by this cut are similar in nature and magnitude to those of the (001)-cut exhibited in the previous figures, showing the domination of the effects of the quasi-transverse waves in all anisotropic phenomena. Fig. 6(a) is similar to Fig. 3(a) for the (001)-cut, the main difference being in the magnitude of the transmitted *qSH* wave which is reduced by about 50 per cent. Fig. 6(b), however, for an incident *SH* wave shows no diminishing of the magnitude of the *qSV* wave, when compared with Fig. 3(c) for the (001)-cut.

For the (100)-cut, the *qP* velocity anisotropy is similar to that of the (101)-cut, but the anisotropy of the quasi-transverse waves is much less (Crampin 1977). Fig. 7(a), for an incident *P* wave, shows little azimuthal variation and the magnitude of the transmitted *qSH* wave is similar to that in Fig. 6(a) for the (010)-cut. Fig. 7(b) shows strong coupling between the incident *SV* wave and the transmitted *qSH* wave only for near normal angles of incidence. This is due to the polarizations of the quasi-transverse waves being nearly along the crystallographic axes for high angles of incidence.

As a model more representative of the velocity anisotropy of the upper mantle as now observed at the surface, we have taken the transversely isotropic medium in Table 1 with the symmetry axis parallel to the surface, and the isotropic half-space, medium 4 in Table 2. Fig. 8(a), (b) and (c) show the behaviour for this model. For the incident *P* wave there is a critical angle for one of the orientations and the transmitted *qSH* wave is quite small. However, for the incident *SV* and *SH* waves the strong coupling with both transmitted quasi-transverse waves still exists.

4 Group velocity directions

In anisotropic media the group velocity of plane waves is not parallel to the propagation vector, and the group direction will be out of the incident plane unless this plane is one of elastic symmetry. The angle ϕ, Fig. 9(a), measures the deviation from plane of incidence and θ_g, Fig. 9(b), is the projection of the group direction on the plane of incidence. θ_p is the direction of the propagation vector. We call the angle θ_g the refraction angle of the group

velocity in the incident plane, θ_p the refraction angle of the phase velocity, and $(\theta_g - \theta_p)$ the deviation of the group velocity from the phase velocity.

Fig. 10(a) and (b) plot these angles for an incident *P* wave from a high-velocity isotropic half-space on the (001)-cut of olivine, corresponding to the structure for Fig. 3(a). Fig. 10(a) illustrates the effect of the velocity anisotropy in the variation of the group velocity refraction angle with orientation. The right-hand graph has only three curves because no *qSH* wave is transmitted for incident planes of symmetry. For non-symmetry planes of incidence the propagation of energy diverges out of the incident plane by up to 20 degrees. The angles ϕ are related to the rates of change of the propagation velocities for each type of wave. The rates of change of some quasi-transverse wave velocities for olivine exhibit a change of sign between symmetry directions. In such cases, ϕ will be positive for some orientations and negative for others as in Fig. 10(a). The *qP* velocities change monotonically between symmetry directions and ϕ for *qP* is always positive or negative.

Fig. 10(b) shows the deviation of the group velocity $(\theta_g - \theta_p)$ and the magnitudes of the group velocities of the transmitted waves.

Fig. 11(a) and (b) are for the same structure but for an incident *SV* wave. The plots for the 45° orientation show the change in nomenclature of *qSV* and *qSH*. The figures are otherwise similar to those for an incident *P* wave except that there is the added complication of the existence of critical angles. Thus the group velocity refraction angle of the transmitted *qP* wave becomes 90° at the critical angle and the group velocity of the 'transmitted' *qP* wave plotted beyond the critical angle is the group velocity of the associated inhomogeneous wave tied to the boundary. Figs 10 and 11 seem typical of the cases we have examined, although there is considerable variation of the magnitudes of the angles.

Conclusion

In comparison with reflection and transmission in isotropic media, the presence of anisotropy complicates the situation in three ways:

(1) The change of velocity with azimuth and with angle of incidence causes variations in the refraction angles, critical angles and amplitudes of the transmitted waves with the direction of orientation.

(2) The variation of polarization introduces converted *qSH* motion for all types of incident waves: *P, SV,* and *SH*. The generation of *qSH* by incident *P* waves is comparatively small, because the *qP* waves usually have small transverse components of motion and most of the energy is converted to *qP*. However, incident transverse waves result in considerable anomalies in comparison with isotropic motion. The cross-coupling of *SH* and *SV* motion may be strong for incident shear waves because the particle motion of *qSH* and *qSV* is fixed by the anisotropy, and not the polarity of the incident wave. In some directions the fixed particle motion of quasi-transverse waves is intermediate between *SV* and *SH* motion, and incident *SV* (or *SH)* waves can, for some orientations, convert into approximately equal amounts of *qSV* and *qSH* energy.

(3) The energy transport diverges out of the incident plane by as much as 20° for some orientations of olivine.

These three types of anomaly are not independent, each one implies the other two. However, as far as one can separate them, it appears that the magnitude and character of the polarization anomalies of body waves are the most diagnostic of anisotropy. Crampin (1975) found that the polarization anomalies of surface waves were also most diagnostic of anisotropic layering.

Acknowledgments

The work undertaken by SC was part of the research programme of the Institute of Geological Sciences, and is published with approval of the Director, IGS.

References

Bamford, S. A. D., 1973. Refraction data in Western Germany – A time-term interpretation, *Z. Geophys.* **39**, 907–927.

Berry, M. J. & Fuchs, K., 1974. Crustal structure of the Superior and Grenville Provinces of the North Eastern Canadian Shield, *Bull. seism. Soc. Am.*, **63**, 1393–1432.

Cerveny, V., 1972. Seismic rays and ray intensities in inhomogeneous anisotropic media, *Geophys. J. R. astr. Soc.*, **29**, 1–13.

Crampin, S., 1966. Higher modes of seismic surface waves: propagation in Eurasia, *Bull. seism. Soc. Am.*, **56**, 1227–1239.

Crampin, S., 1967. Coupled Rayleigh–Love second modes, *Geophys. J. R. astr. Soc.*, **12**, 229–235.

Crampin, S., 1970. The dispersion of surface waves in multilayered anisotropic media, *Geophys. J. R. astr. Soc.*, **21**, 387–402.

Crampin, S., 1975. Distinctive particle motion of surface waves as a diagnostic of anisotropic layering, *Geophys. J. R. astr. Soc.*, **40**, 177–186.

Crampin, S., 1977. A review of the effects of anisotropic layering on the propagation of seismic waves, *Geophys. J. R. astr. Soc.*, **49**, 9–27.

Crampin, S. & King, D. W., 1977. Evidence for anisotropy in the upper mantle beneath Eurasia from the polarization of higher mode seismic surface waves, *Geophys. J. R. astr. Soc.*, **49**, 59–85.

Crampin, S. & Taylor, D. B., 1971. The propagation of surface waves in anisotropic media, *Geophys. J. R. astr. Soc.*, **25**, 71–87.

Francis, T. J. G., 1969. Generation of seismic anisotropy in the Upper Mantle along the mid-oceanic ridges, *Nature*, **221**, 162–165.

Hess, H., 1964. Seismic anisotropy of the uppermost Mantle under oceans, *Nature*, **203**, 629–631.

Keith, C. M., 1975. Propagation of seismic body waves in layered anisotropic structures, *PhD dissertation*, Edinburgh University.

Raitt, R. W., Shor, G. G., Francis, T. H. G. & Morris, G. B., 1969. Anisotropy of the Pacific Upper Mantle, *J. geophys. Res.*, **74**, 3095–3109.

Raitt, R. W., Shor, G. G., Morris, G. B. & Kirk, H. K., 1971. Mantle anisotropy in the Pacific Ocean, *Tectonophys.*, **12**, 173–186.

Synge, J. L., 1956. Flux of energy for elastic waves in anisotropic media, *Proc. Roy. Irish Acad. A.*, **58**, 13–21.

Synge, J. L., 1957. Elastic waves in anisotropic media, *J. Math. Phys.*, **35**, 323–335.

Verma, R. K., 1960. Elasticity of some high density crystals, *J. geophys. Res.*, **65**, 757–766.